Asian Power Electronics Journal

PERC, HK PolyU

First edition August 2021 Printed in Hong Kong by Reprographic Unit.
The Hong Kong Polytechnic University

Published by
Power Electronics Research Centre
The Hong Kong Polytechnic University
Hung Hom, Kowloon, Hong Kong

ISSN 1995-1051

Disclaimer
Any opinions, findings, conclusions, or recommendations expressed in this material/event do not reflect the views of The Hong Kong Polytechnic University

Editorial board

Table of Content

A Study of LLC Converter with Buck Converter for CC-CV Charging

H.K.T. Tsang, Y.C. Fong, Kin Lung Jerry KAN, S. Raghu Raman, K.W.E Cheng

Power Electronics Research Centre, Department of Electrical Engineering, The Hong Kong Polytechnic University, Hong Kong
E mail: hon-ki.tsang@polyu.edu.hk

Abstract – For having switching frequency equal to resonant tank frequency in LLC converter, a unity voltage gain can be achieved over the entire loading conditions but it is not suitable for the Constant Current-Constant Voltage (CC-CV) battery application. Also, the voltage gain characteristic of LLC converter is frequency dependent. For battery charging application, a wide range of switching frequency is required for supplying constant current, charging the battery with its varying load characteristic. It causes above and below resonant frequency operation which causes losses and noise. As result, it is proposed to make use of a buck converter at the output of LLC converter for regulating the charging current and voltage for battery charging application.

Keywords - LLC converter, Buck converter, CC-CV battery charging, closed-loop control

I. Introduction

For on-board charger, it is common to use a resonant converter for providing the isolation for safety and high output power level by employing a resonant tank [1]. One of the well-known topologies is the full-bridge LLC converter with a full-bridge rectifier. Its construction is simple because only a resonant capacitor is required for resonating with the leakage inductance of the high-frequency transformer. By using the inherent leakage inductance of the transformer, a resonant inductor can be eliminated. Cost and component count can be reduced.

A complicated control scheme, such as variable frequency control, is inevitably adopted an LLC converter [2]. Other advanced control schemes for applying to the wide-range input voltage and/or output voltage application can be found also [3]. However, for this paper application, the input voltage is fixed to 220Vac/50Hz rectified to 312Vdc, there is no need for the design of the LLC converter to take into consideration of a wide range of input voltage. In that case, it is chosen to use fixed frequency switching for the LLC converter with open-loop control, cascaded with a buck converter at its output, for regulating the charging current and voltage in CC-CV battery charging. It will be an easy implementation for a CC-CV battery charger.

Apart from that, using a buck converter simplifies the design of the LLC converter. For a typical LLC converter design, it is required to optimize the ratio of leakage inductance with magnetizing inductance for the high-frequency transformer [4]. This design procedure can be saved so that it is only required for choosing the resonant frequency of the resonant tank. With fixed switching frequency in the LLC converter as resonant frequency, its output voltage will be fixed independent of load condition. And it can be regulated by the duty cycle of the buck converter, for CC-CV battery charging.

For a LLC converter, the resonant capacitor will be selected for resonating with the leakage inductance of the LLC transformer. Its capacitance owns tolerance which will cause the failure of resonant condition of the LLC converter [5]. As a result, the output voltage of LLC converter may not be load-independent. By using buck converter for regulating the output of LLC converter, it allows the variation of the output voltage from the LLC converter, ensures CC-CV charging.

One more advantage of using buck converter is that, as mentioned before, the requirement for the transformer design of the LLC converter is released. So, it allows the primary winding and secondary winding of the transformer wound on two separate ferrite cores. It gives the chance for making a contactless connector for Electric Boat charger. Because when an electric boat lies at the pier, people concerns about getting an electric shock near the water when charging a boat by a metal-conductive charger connector. As a result, it will be a good use if a contactless charger connector can be made.

This paper is organized into three sections, Section II gives the modeling of LLC converter for estimating the output voltage variation, Section III gives a simulation model of overall circuit performance for showing the CC-CV mode charging. Section IV gives the experiment setup for showing the performance of the LLC converter with buck converter.

II. Modeling of LLC Converter in Resonant State

A typical circuit of a full-bridge LLC converter with a full-bridge rectifier is shown in Fig. 1 [4].

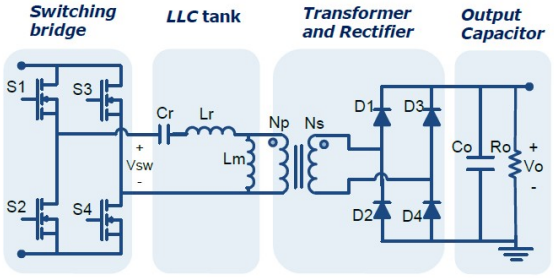

Fig. 1: Circuit connection of a full-bridge LLC converter with full-bridge rectifier [4]

By optimization, the equivalent circuit of Fig. 1 can be obtained as shown in Fig. 2 [4].

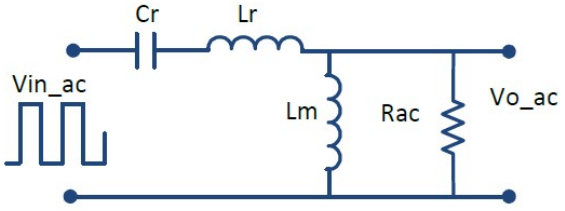

Fig. 2: Equivalent circuit of a full-bridge LLC converter with full-bridge rectifier [4]

From Fig. 2, the magnitude of the output-input voltage ratio of the equivalent circuit can be derived as shown in Eqn. (1) [4].

$$K(Q,m,F_x)=\left|\frac{V_{o\_ac}(s)}{V_{in\_ac}(s)}\right|=\frac{F_x^{\,2}(m-1)}{\sqrt{\left(m\cdot F_x^{\,2}-1\right)^2+Fx^2\cdot\left(F_x^{\,2}-1\right)^2\cdot(m-1)^2\cdot Q^2}} \quad (1)$$

Where,

$Q=\frac{\sqrt{L_r/C_r}}{R_{ac}}$ Quality factor

$R_{ac}=\frac{8}{\pi^2}\cdot\frac{N_P^{\,2}}{N_S^{\,2}}\cdot R_o$ Reflected load resistance

$F_x=\frac{f_s}{f_r}$ Normalized switching frequency

$f_r=\frac{1}{2\pi\sqrt{L_r\cdot C_r}}$ Resonant frequency

$m=\frac{L_r+L_m}{L_r}$ Ratio of total primary inductance to resonant inductance

Based on Eqn. (1), the magnitude of voltage gain is plotted under the circuit parameters shown in Table 1.

Table 1: Circuit Parameters

Circuit Parameters	value
Resonant inductance, L_r	562uH
Resonant capacitor, C_r	4.7nF
Resonant frequency, f_r	100kHz
Magnetizing inductance, L_m	1.37mH
Turns ratio, Np:Ns	76:78
R_o	11.25Ω to 19.125Ω

For the R_o range, this application is going to supply a lithium battery with 144V/80Ah capacity. The constant charging current is selected to be 8A, and the minimum voltage of the battery is set to 90V, the constant voltage charging is selected to be 153V. As a result, R_o will be in the range of 11.25Ω to 19.125Ω under CC mode.

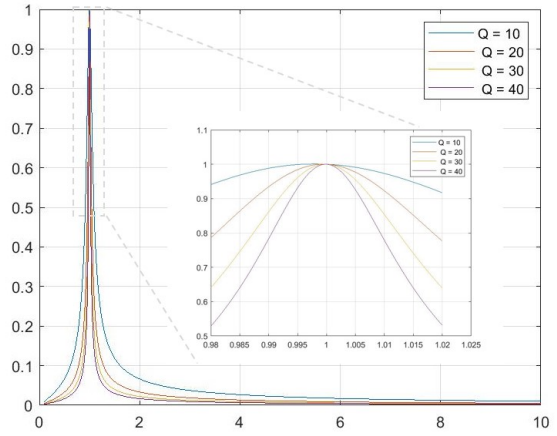

Fig. 3: Magnitude of Output-input voltage gain curve

From Fig.3, it is shown that when switching frequency is the same as resonant frequency (F_x = 1), no mater under which load condition, the voltage gain remains to be 1. Then, for the buck converter, the LLC converter behaves as a fixed output voltage source. The buck converter is controlled by varying its duty cycle for the CC-CV charging battery.

III. Simulation of LLC Converter with Buck Converter

A. LLC converter only

A simulation model is created by the software PSIM™ as shown in Fig. 4. Fig. 5 shows the fixed output voltage characteristic of the LLC converter when f_s = f_r. It is observed that the output voltage of the LLC converter is independent of load condition. Fig. 6 shows the H-bridge output voltage and current under R_0 = 11.25Ω and R_0 = 19.125Ω, in an open loop control for 1:1 fixed output voltage. The resonant state of the LLC converter is achieved.

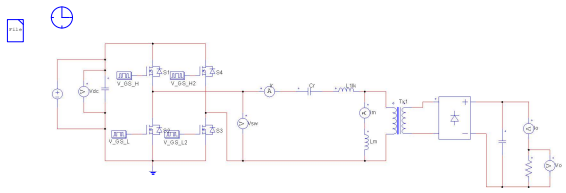

Fig. 4: Simulation model of the full-bridge LLC converter with full-bridge rectifier

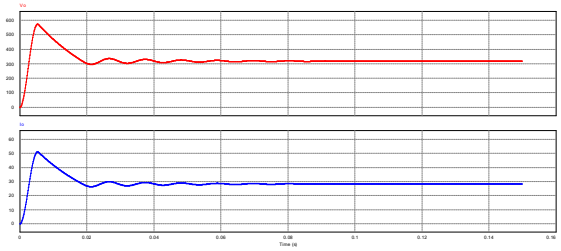

(i)

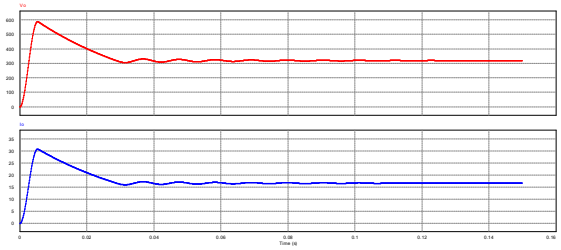

(ii)

Fig. 5: Output voltage and output current simulation result (i) R_o = 11.25Ω (ii) R_o= 19.125Ω, under open loop condition

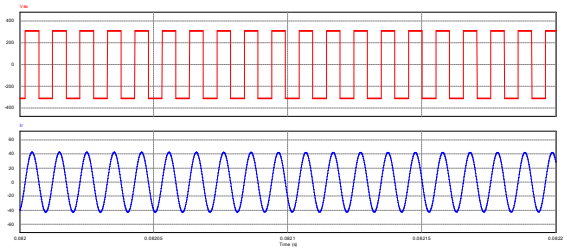

(i)

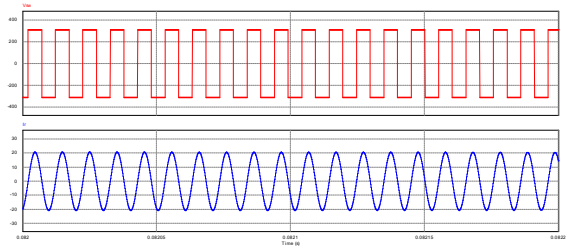

(ii)

Fig. 6: The H-bridge output voltage and current simulation result (i) R_o = 11.25Ω (ii) R_o= 19.125Ω, under open loop condition

B. LLC converter with buck converter in closed-loop form

Under the closed-loop control, a simple comparator circuit of inductor current and output current comparison, is implemented. Fig. 7 shows the simulation model based on the circuit parameter defined in Table 2 for the buck converter. Fig. 8 shows the output voltage of LLC converter, charging voltage and charging current when (i) R_o = 11.25Ω, (ii) R_o= 19.125Ω. Fig. 9 shows the H-bridge output voltage and current under R_0 = 11.25Ω and R_0 = 19.125Ω, in a closed loop control for 8A output current. The resonant state of the LLC converter is achieved.

From the simulation results, it is proved that under $f_s = f_r$, the buck converter is getting a fixed input voltage at its input side. As a result, the buck converter does not require to adapt a wide range of input voltage and no need for a complicated control scheme.

Table 2: Circuit Parameters for the Buck converter

Circuit Parameters	value
Inductor, L	550uH
Input capacitor, C_{in}	100uF
Switching frequency, f_r	100kHz
Output capacitor, C_{out}	330uF

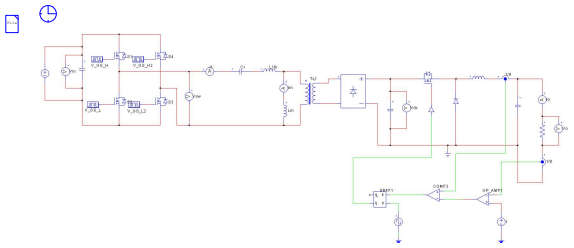

Fig. 7: Simulation model of LLC converter with Buck converter in closed-loop form

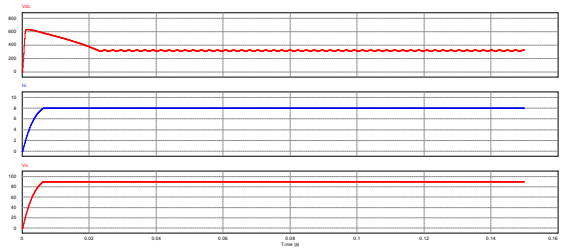

(i)

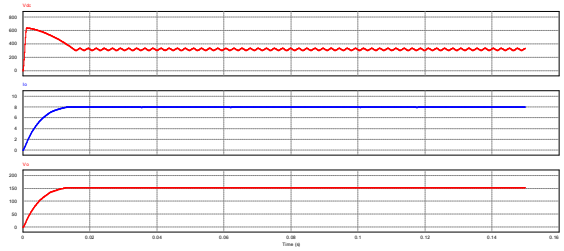

(ii)

Fig. 8: Output voltage of LLC converter, output voltage and output current simulation result (i) R_o = 11.25Ω (ii) R_o= 19.125Ω, under closed loop condition

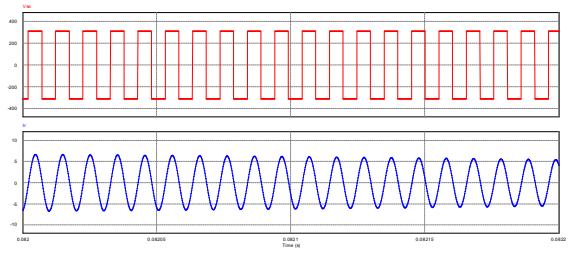

(i)

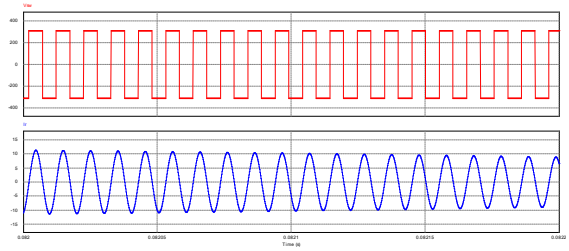

(ii)

Fig. 9: The H-bridge output voltage and current simulation result (i) Ro = 11.25Ω (ii) Ro= 19.125Ω, under closed loop condition

C. LLC converter with buck converter in control of C code

Under the closed-loop control, it is inevitable for using C code to control the switching mode of the CC-CV mode charging. In the simulation model, a C program block was used to emulate the microcontroller which controls the charger operation. The CC-CV mode charging operation was implemented with PI compensation according to the voltage and current feedback. Fig. 10 shows the simulation model based on the design of C code. Fig. 11 shows its output voltage and output current. It is proved that the program is worked for switching the converter to CV code with decreasing output current.

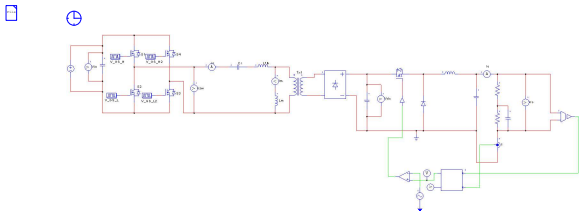

Fig. 10: Simulation model of LLC converter with Buck converter in closed-loop form by C code

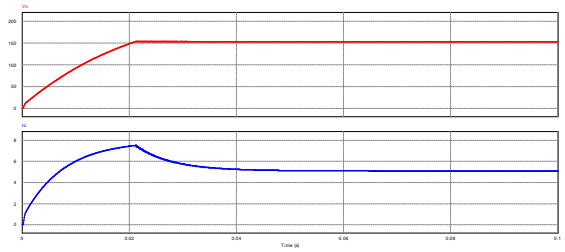

Fig. 11: The output voltage and current simulation result, under closed loop control by C code

IV. EXPERIMENTAL RESULTS OF THE PROPOSED CIRCUIT

A buck converter prototype is built and shown in Fig. 12. Experimental waveforms at CC mode current = 6A and 8A are shown in Fig.13. Table 3 shows the efficiency of the buck converter. Under the constant current charging at 8A, the buck converter can achieve 96.5% efficiency.

Fig. 14 shows the separable primary and secondary winding for using the high-frequency transformer of the LLC converter, its parameter as shown in Table. 1. The conductors of the split-core transformer and the coupling point are completed sealed. This design aims to be used in a water environment for charging eliminating the risk of electric shock.

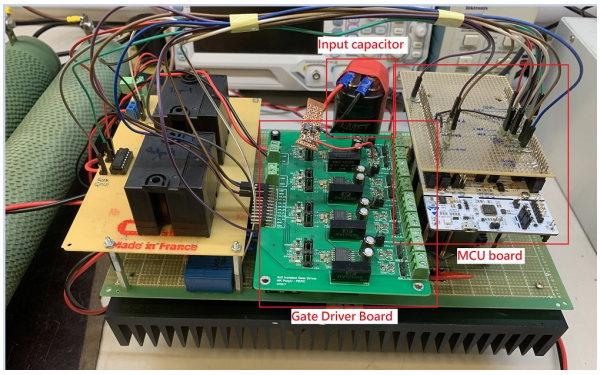

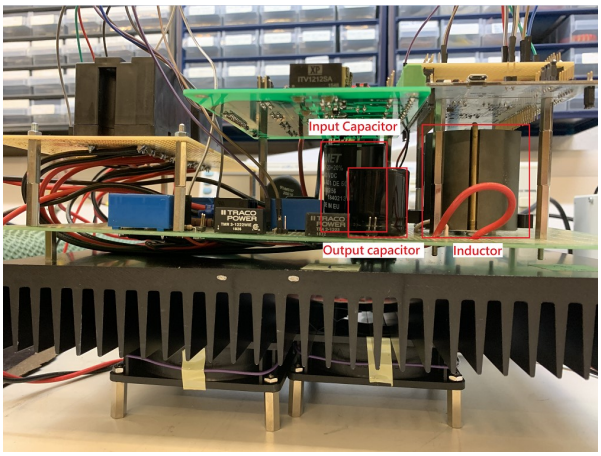

Fig. 12: A prototype of the buck converter

(i)

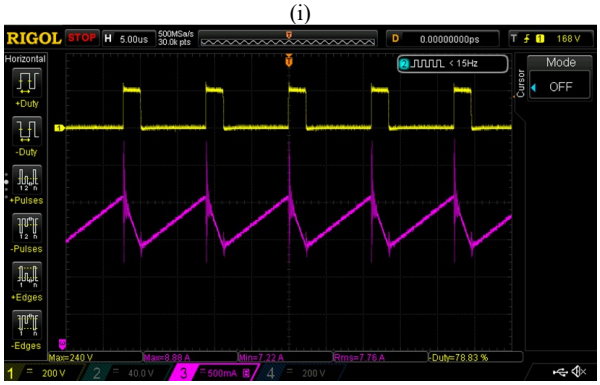

(ii)

Fig. 13: Drain-source voltage of high side MOSFET and inductor current waveforms (i) CC mode current = 6A (ii) 8A

Table 3: Efficiency of the Buck converter

CC mode current	P_{out}	P_{loss}	Eff.
2A	77W	10W	88.5%
4A	310W	20W	94.0%
6A	691W	39W	94.7%
8A	1141W	42W	96.5%

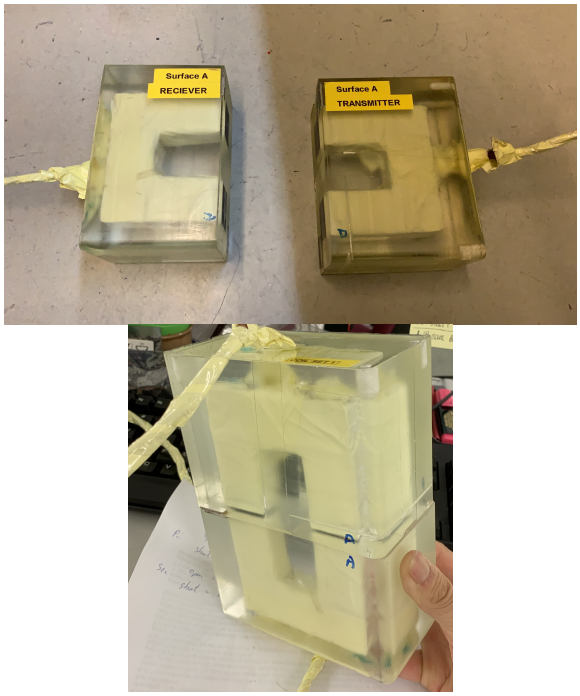

Fig. 14: Separable primary and secondary winding used in the LLC converter

V. Conclusion

This paper presents an LLC converter with a buck converter for CC-CV charging. The simulation and prototype are presented for proving that the idea is achievable and attains the highest efficiency at 96.5%. Besides, the hardware of the separable primary and secondary winding for using as a high-frequency transformer of the LLC converter is demonstrated for showing the possibility of producing a water-proof connector for battery charging application under water.

References

[1] J. Zeng, G. Zhang, S. S. Yu, B. Zhang and Y. Zhang, "LLC resonant converter topologies and industrial applications — A review," in Chinese Journal of Electrical Engineering, vol. 6, no. 3, pp. 73-84, Sept. 2020.

[2] P. Kowstubha, K. Krishnaveni and K. Ramesh Reddy, "Review on different control strategies of LLC series resonant converters," 2014 International Conference on Advances in Electrical Engineering (ICAEE), Vellore, 2014.

[3] G. Liu, Y. Jang, M. M. Jovanović and J. Q. Zhang, "Implementation of a 3.3-kW DC–DC Converter for EV On-Board Charger Employing the Series-Resonant Converter With Reduced-Frequency-Range Control," in IEEE Transactions on Power Electronics, vol. 32, no. 6, pp. 4168-4184, June 2017.

[4] "Resonant LLC Converter: Operation and Design 250W 33Vin 400Vout Design Example", AN2012-09, Sam Abdel-sRahman, Infineon Technologies North America (IFNA) Corp.

[5] H. Vu and W. Choi, "A Novel Dual Full-Bridge LLC Resonant Converter for CC and CV Charges of Batteries for Electric Vehicles," in IEEE Transactions on Industrial Electronics, vol. 65, no. 3, pp. 2212-2225, March 2018.

Electric Waterjet Thruster Vessel Development – Concept, Charger, and Battery Monitoring

Kin Lung Jerry Kan[1] , Y.C. FONG[2] , IP Shu Chuen[3] , H.K.T. Tsang[4] , H.F. Ho[5] , X.D. Xue[6] , Y.L. Fan[7] , K.W.E. Cheng[8]

Power Electronics Research Centre, The Hong Kong Polytechnic University, Hong Kong
[1]E-mail: jerry.kan@connect.polyu.hk, [2]E-mail: yat-chi.fong@polyu.edu.hk, [3]E-mail: shu.ip@polyu.edu.hk,
[4]E-mail: hon-ki.tsang@polyu.edu.hk, [5]E-mail: james.ho@polyu.edu.hk, [6]E-mail: xd.xue@polyu.edu.hk,
[7]E-mail: yulong.fan@polyu.edu.hk, [8]E-mail: eric-cheng.cheng@polyu.edu.hk.

Abstract— This paper exhibits an overall design of an electric waterjet vessel. Marine craft electrification especially the propulsion system transfer from the diesel engine to electric switched reluctance motor realizes the environmental-friendly utilization. A corresponding waterproof inductive wireless charger which could operate under water-immersed condition is introduced to prompt higher marine craft electrical penetration. This work presents the first development of a novel design of a marine charging system on a jet boat environment for lower power application. The use of near field magnetic transfer lifts the power conversion efficiency and at the same time, improves the safety and reliability of the charging operation. The system has been built and tested successfully to validate the concept boat.

Keywords— Marine electrification, Waterproof inductive charger, switched reluctance motor-driven waterjet.

I. INTRODUCTION

Ideally the diesel engines have high fuel energy density which is almost 181g fuel/kWh that suits the transportation application well. However, the vessels have various operation mode. The standby mode and relocation a boat is on boarding progress representing an extreme low load condition which drags the fossil fuel generator performance [1]. Furthermore, the motor driven propeller and waterjet bow thruster propulsion system enable the regenerative braking and energy generation which boosts the system efficiency. The e-ferry energy cost performance 0.11$/kWh has 13 times higher than the diesel engine around 1.38$/kWh upon the entire service scenarios [2].

The diesel combustion engine emission problems bring great concern on the environmental protection. International Marine Organisation (IMO) posed restricts on the exhaust emission value of oxides of nitrogen. For the engine maximum operation speed (n/rpm) over 2000, the NO_X emissions limits should be 1.96g/kWh from 2016 at the NO_X emission-controlled area (ECA) and globally 7.7g/kWh. The sulphur limit value is 0.1% (m/m) in SO_X-ECA while the corresponding content is 0.5% (m/m) on global from 2020 [3]. Obviously there are three methods: 1. retire the unqualified craft, 2. replace or improve the diesel engine on existing boat, 3. implement the new generation vessel such as e-ferry driven by battery which is exhaust emission free. In addition, there are oil residue, operation noise to ambient environment comprises of onshore and underwater. Flaws result in numerous ecology catastrophe. Dylejko presented the total radiated noise levels of marine diesel engines with different vibration isolation system maintain from 98dB to 140dB under 1kHz [4]. 2016, US National Marine Fisheries Service (NOAA) issued a marine mammal guidance to regulate the vessel acoustic thresholds by marine mammal auditory weighting function. The non-impulsive receiving level of the ferry should be 120dB and impulsive is 160dB [5]. Fig. 1 reveals, in light of the relative silent operation motor and the intrinsic enclosure impeller structure, battery-motor-driven waterjet propulsion system mitigates the load noise, marine fauna amputations cause by propeller [6] and the complicated combustion engine ducts mechanism.

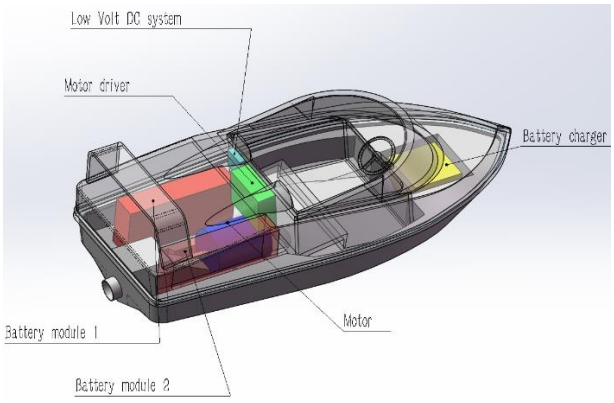

Fig.1 Propulsion system profile

The conventional e-ferry battery charging method is conductive charging with a metal plug. However, coastal ferries operate outdoor and always in a harsh and saline environment which challenges electrical safety. In the latest marine wireless charging application, there is a 1-MW inductive charging system in Norway [7]. The fixed installation makes it only suit the regular route cruise and the harbour with high power capacity. In a wide fjord area, the power grid is not strong. A pre-charged power dock consisted of the battery is an alternative method for high power transfer which can provide a 20-min fast charge [7]. But the expense of battery limits the e-ferry transportation cover area. High mobility and a user-friendly charger would be essential for the mass electrification of small vessels. An all insulated, small in size and 13-A socket applicable wireless charger is in desire.

This paper presents the propulsion, control, and energy storage system electrification. Section II introduces the propulsion system of the waterjet engine including the battery, motor, and waterjet characteristics. A magnetics-based all-insulated inductive wireless charger is illustrated

in section III. In section IV, the onboard DC distribution is presented briefly. Section V exhibits the experiments to validates the proposed concept.

II. Propulsion System & Battery

1. Waterjet pump operation profile

Pumps of waterjet are classified as axial flow, mixed flow, and centrifugal flow pumps for the angles of inflow and outflow [8]. Fig.2 reveals a common and typical mixed flow impeller pump for the waterjet engine. The waterjet engine propulsion system is composed of the inlet duct, impeller, driveshaft, stator, and nozzle. The rotating impeller driven by the shaft generates the thrust to provide the propulsion force with a directional control nozzle. Driveshaft coupled with the switched reluctance motor (SRM) in this case. SRM is very suitable for the marine and ship application for high operation performance [9]. Propulsion force provided by the waterjet engine is decided by the mass flow experienced in the impeller and the water leave velocity from the nozzle:

$$\dot{m} = \rho A_2 V_2 \tag{1}$$

where ρ is the sea water density, A_2 is the outlet duct area. Hence, the thrust T could be acquired by the rate of the water momentum changes through the nozzle, and the propulsion power P_p is:

$$T = \dot{m}(V_2 - V_1) = \rho A_2 V_2 (V_2 - V_1) \tag{2}$$

$$P_p = TV_S \tag{3}$$

The propulsive performance η_D could be determined by the cascaded efficiency formula [10]:

$$\eta_D = \eta_H \, \eta_O \eta_R \eta_C \eta_M \tag{4}$$

where η_H is the hull efficiency which indicates the power transfer from all propulsors to the hull traction power. η_O exhibits thrust power performance of the impellers. The impeller operation efficiency various from the open water condition to actual condition that η_R is given to amend it. η_C, η_M are the shaft coupler efficiency and the motor efficiency.

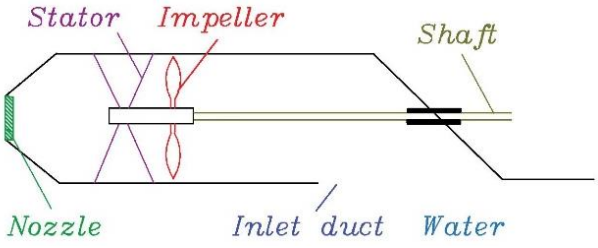

Fig.2 Waterjet thruster structure

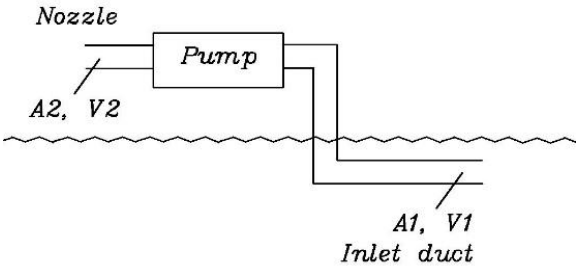

Fig.3 Idealized waterjet thruster arrangement

2. Switced reluctance motor designing

The SRM installation conducted as Fig.4. compared with the fossil fuel engine, it is more silent to drive and reduces the vibration caused residual resistance and skin friction resistance. There is a trade-off between the high power and less weight of the motor. Less weight eases the immersive of the hull which reduces much resistance. Fig.5 proposes an SRM design flowchart.

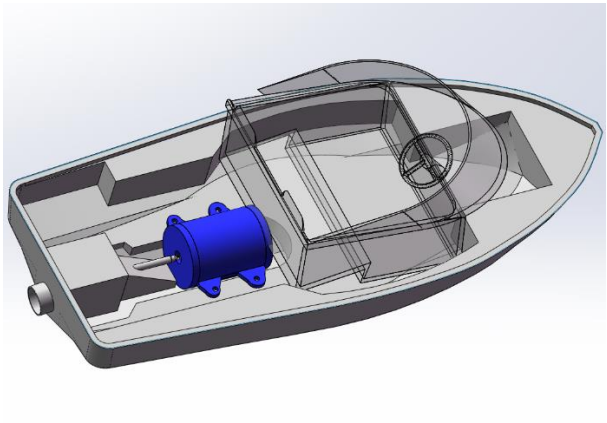

Fig.4 SRM installation position.

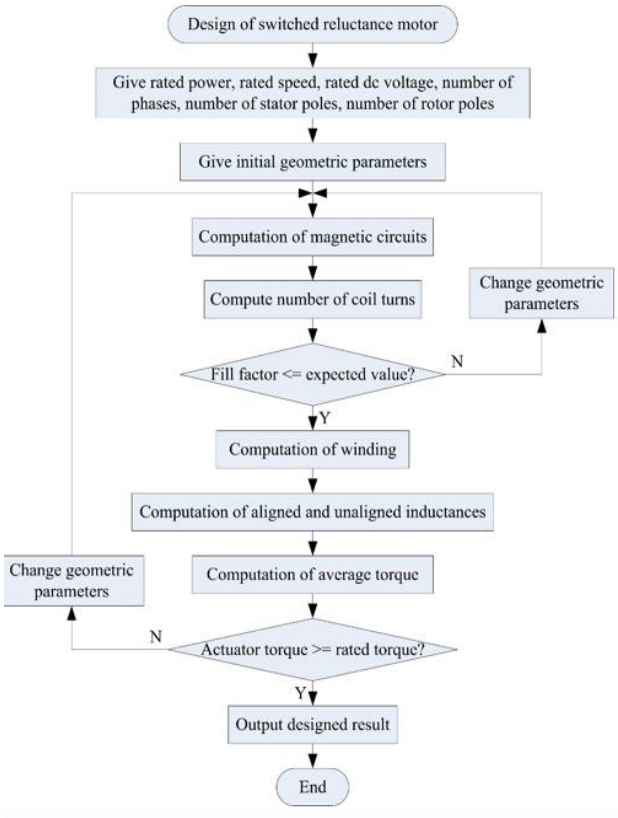

Fig.5 SRM design flow chart.

3. Lithium ion phosphate battery

Though the Lithium-ion phosphate (LFP) battery has approximately 10-30% energy density lower than the other lithium battery, the concern of safety and environment makes it a suitable choice. LFP is a cobalt-free Lithium battery, it reduces the pollution to the environment even battery sunk to the water. The difficulty in the ignition even at charging or short circuit circumstances make it a feasible power source on board.

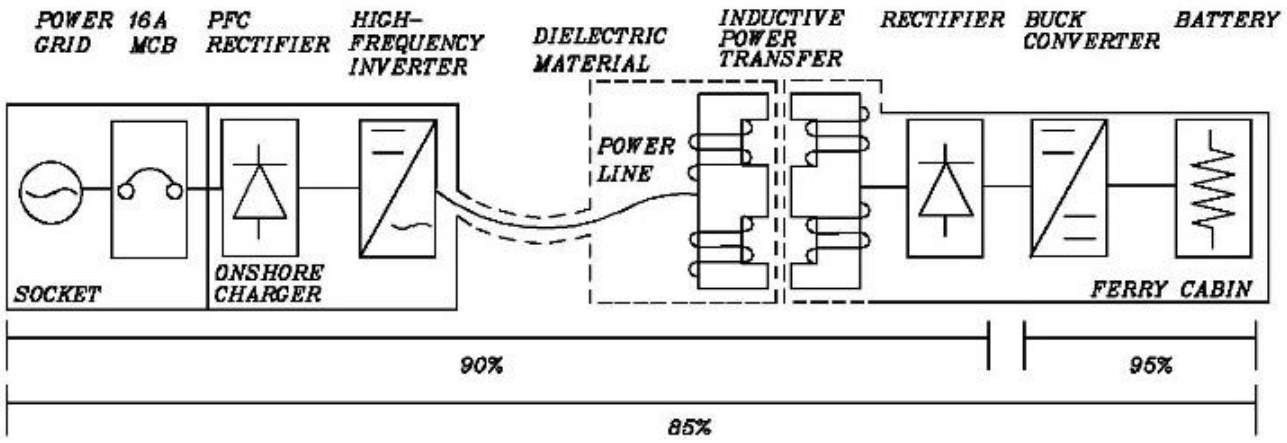

Fig.6 A standard LLC WPT system with 85% overall efficiency

III. All Insulated Wireless Charger

Inductive power transfer through the time-vary magnetic field guarantees a high-efficiency wireless power transfer. A well-insulated coil generates a high-frequency magnetic field for vessel battery charging does not have any electric shock hazard to the creature. Both transmitter and receiver of the charging system covered by dielectric material prevent the potential risk of conductive charging with metal contacts.

LLC resonance circuit offers a high efficiency inverting technique for wireless charging. Fig.7 is a typical LLC converter topology and the transformer Tx could be primary and secondary side separated to form the metal-free power transfer. The primary side acts as a transmitter while the secondary side performs as a receiver. The merit of LLC circuit is the zero-voltage switching (ZVS). The concept is that before the switch turns on, the reverse diode conducts so that the switching voltage is set as the diode forward voltage which should be a relatively low value. The key measure is to set the switching frequency in the vicinity of the resonance frequency:

$$f_0 = \frac{1}{2\pi\sqrt{L_r C_r}} \tag{5}$$

$$f_n = \frac{f_{sw}}{f_0} \tag{6}$$

The loop inductance and the leakage inductance of the charging loop constitute the resonance inductance L_r. A capacitor C_r is deployed to generate the alternative current from DC in the full-bridge circuit. First Harmonics Approximation (FHA) is an effective way to estimate and design the circuit parameter. V_{oe} is the equivalent output voltage of the LLC circuit. L_m is the magnetizing inductance between the WPT transmitter and hull receiver while L_r represents the resonant inductance of wire parasitic inductance, transformer leakage inductance and power line loop inductance. C_r is the compensation capacitor.

$$\dot{V_{oe}} = \frac{2V_{DC}\sin(2\pi f_{sw}t)}{\pi} \tag{7}$$

$$V_{oe\_rms} = \frac{V_{in}}{\pi\sqrt{2}} \tag{8}$$

$$I_{oe\_rms} = \frac{\pi I_o}{n2\sqrt{2}} \tag{9}$$

$$R_e = \frac{V_{oe\_rms}}{I_{oe\_rms}} = \frac{8n^2}{\pi^2} R_{load} \tag{10}$$

Therefore, the equivalent quality factor Q_e could be estimated:

$$Q_e = \frac{\sqrt{\frac{L_r}{C_r}}}{R_e} \tag{11}$$

$$M_g = \frac{V_{oe}}{V_{ge}} = \left|\frac{jX_{Lm} \parallel R_e}{(jX_{Lm} \parallel R_e) + j(X_{Lr} - X_{Cr})}\right|$$

$$= \left|\frac{L_n f_n^2}{[(L_n+1)f_n^2 - 1] + j[(f_n^2 - 1)f_n Q_e L_n]}\right| \tag{12}$$

$$V_o = \frac{M_g V_{in}}{n} \tag{13}$$

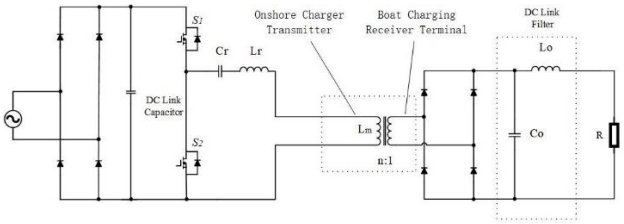

(a)

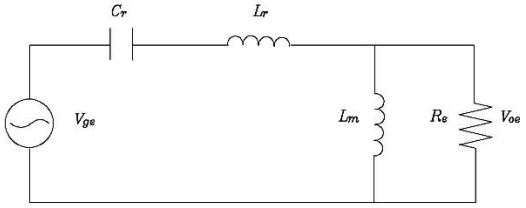

(b)

Fig.7(a) LLC circuit configuration;(b) FHA model

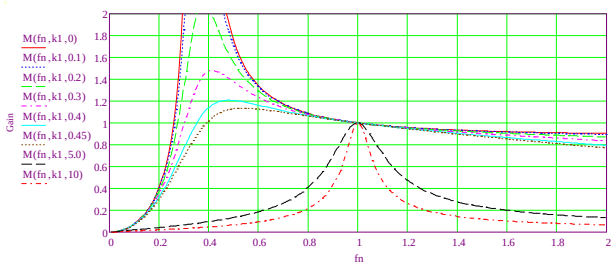

Fig.8 M_g Circuit gain curve

At the conventional LLC converter, one advantage is frequency modulation but not in wireless power transfer (WPT) application. Due to the low-quality factor the WPT configuration, the M_g , LLC converter gain curve with switching frequency varies drastically. Circuit gain changes intensively to maintain a steady output voltage. In Fig.5, the Q_e curves from 0.1 to 0.45 show extremely sharp which is not in compliance with the effective circuit gain control. It is preferred to set at one fix inverter operation switching frequency for power transfer. As to the charging power regulation, a DC/DC converter, for example, a buck converter should be applied to control the output voltage and current level. Constant current (CC) and constant voltage (CV) charging strategy adopted in this prototype. At last, due to the Q_e changes with load, that floats the circuit gain and output voltage. Hence, the full-load no-load output voltage range control should be done prior to circuit design.

IV. Electric Vessel DC Distribution System

Hierarchical control is designed to decouple behaviour between different layers. This improves the over safety of the system [11]. Thereby the proposed network reveals in Fig.9. Battery regulated by a main bidirectional DC/DC converter is useful for the optimal real-time voltage and current of droop characteristics [12]. As mentioned, the busbar voltage level is 150V while the user interface voltage is 36V. The SRM motor signal including the speed, voltage and current data would be recorded by the VCU and to estimate the hull velocity and power consumption with reference of the battery SoC revealing on the panel. The battery regulation converter would be the primary protection of the battery for the unexpected overvoltage from the motor or the insulation fail in the network. The secondary protection is conducted by each inverter or DC/DC converter to cur the fault if overcurrent occurs.

TABLE 1: E-vessel parameter

Hull material	Glass fibre
Capacity	2-person
Rated velocity	18knots
Maximum velocity	26knots
Waterjet type	Mixed flow impeller
Motor type	Switched Reluctance Motor
Motor nominal power	20kW
Motor maximum power	55kW
Power source	LFP battery
Battery voltage range	300V/80Ah
User interface voltage	36V
Busbar voltage	150V

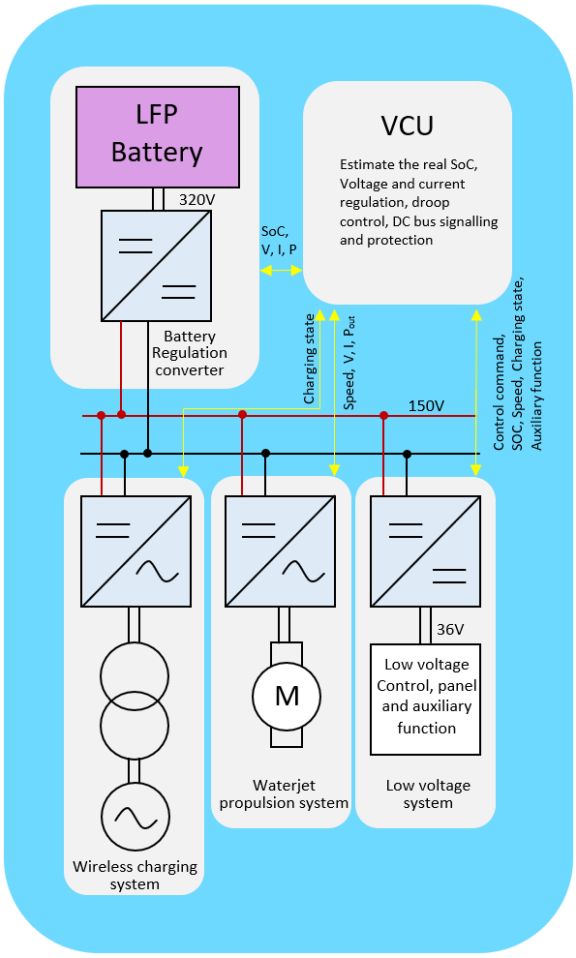

Fig. 9 The proposed DC distribution network for small e-vessel

V. Simulation and Experiment Result

A 1.4kW all insulated inductive wireless charger prototype has been developed to validate the proposed concept. Fig. 10(a) reveals the live coil, ferrite and thermal detector are immersed into the epoxy until to be an integrated structure with the shell. A 9.42mm sq. litz wire implemented to ease the skin effect of charger high frequency operation and avoid the high temperature for the enclose of wire from air. The powerline extended from the charger box to the coil plug is protected by a grounded armoured tube in case of any potential mechanical destroy at the charging spot. Mobile charger transmitter plug was designed with a handle to be plugged on the receiver. The top-edge of the cupped receiver should be fixed on the surface. All the exposure components are water-resistance.

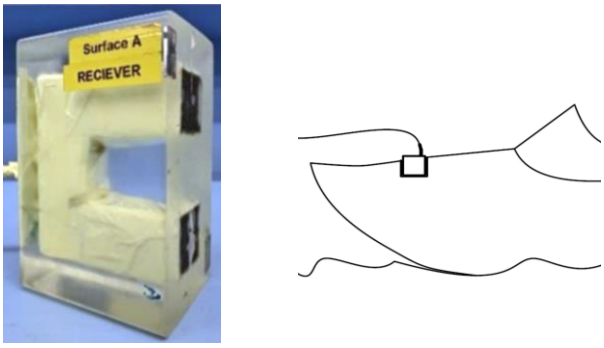

(a) (b)

Fig. 10 (a)Transparent demonstration for the concept of all insulated WPT charger coverd by epoxy. (b)Charging scenario.

(a) (b)

Fig.11 The all-insulated inductive charger

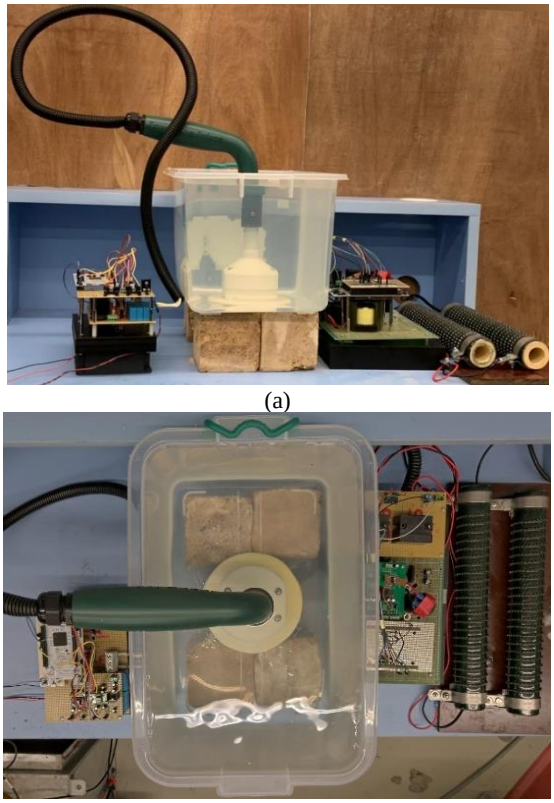

(a) (b)

Fig.12 The proposed all insulated charger tested in water tank (a) front view;(b) top view.

TABLE 2: E-vessel contactless charging system parameter

LLC WPT Charger	
Maximum Power	1.4kW
Input voltage	220V AC
Power line current	13.5A
Receiver input voltage	232V AC
Operation frequency	145kHz
Regulation Buck Converter	
Battery side voltage range	200V to 400V DC
Busbar side voltage range	90V to 153V DC
rated current	8A
Overall system	
Full power operation efficiency	89.3%

As the DC distribution Fig.13, the regulation DC/DC buck converter is connected to the 150 V DC busbar. The charging experiment formed as Fig.12 and the 20 Ω resistance was used to emulate the charging current to the battery. The result indicating on Fig.13(A) shows the drain-source voltage of S4 in Fig.6(a) Resonance current I_r is negative at the moment of S4 is turning on. ZVS achieved owing to the small forward voltage of reverse-diode. Fig.13(b) releases the LLC WPT circuit characteristics of two-port network under full load circumstance which means the starting point of CV charging. The maximum operation efficiency of the LLC WPT charger is 92.6% with 1.4kW input power with sufficient ventilation in the charging box. Fig.14 is the regulation buck converter profile and the power flow from charger to battery management system circuit is 150V busbar DC voltage with 8A charging current.

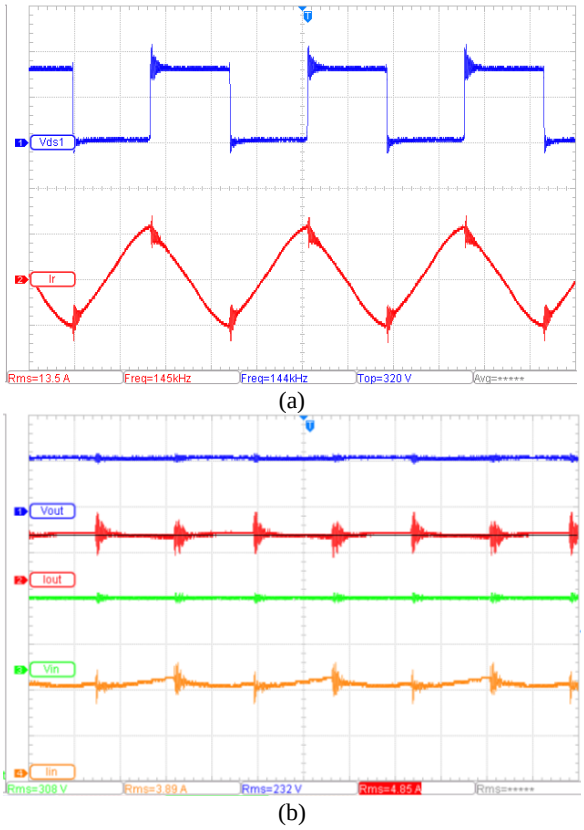

(a)

(b)

Fig.13 (a)ZVS of the full bridge test rig: CH1,S4 MOSFET drain source voltage; CH2, current in power line. (b)Full-load operation. CH1,Output voltage: V_{out_LLC} (200v/div); CH2,output current: I_{out_LLC}(5A/div); CH3,input voltage: V_{in} (200V/div); CH4,input current I_{in}(2A/div);

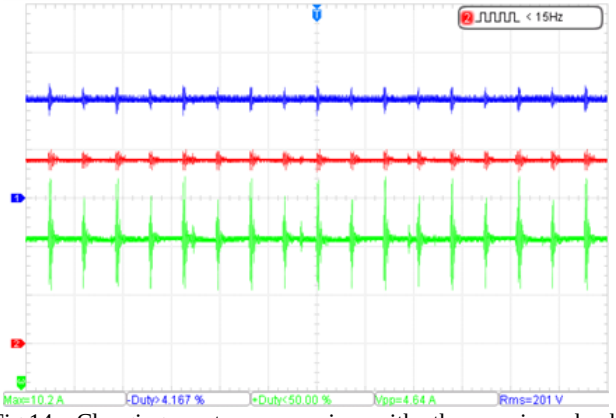

Fig.14, Charging system comprise with the receiver buck converter full power constant voltage charging waveform:CH1,input voltage: V_{out_LLC} (100v/div); CH2,output voltage: $V_{out\_DC\ busbar}$ (40v/div); CH3,output current: I_{out} (2A/div),8A RMS.

A simulation study was conducted to investigate the battery behaviour during sailing. The 300V LFP module was developed based on the study presented in [13]. At various capacities ranged from 40Ah to 80Ah, the SOC as well as the bus voltage profile of the battery pack under loading at different C-rates and constant power of 20kW has been simulated in Fig.15.(a). As shown in Fig.15, the voltage and SOC curves for the case of (2), (5), (8) and (3), (6), (9) at the 1C and 2C discharging rates are overlapped together, which are fully discharged after 1800s and 3600s, respectively. Considering the cases of 20kW constant power discharge, with a 40Ah battery pack, the battery took about 2100s to discharge from the initial voltage of about 312 V to 290 V, whereas when the capacity was double to 80Ah, or approximately 24kWh, the battery pack lasted for more than 4300s. It could also be noted that with large battery size, the case of 80Ah had the lowest initial voltage drop of about 3 V. This implies that the lowest internal resistance could help improve the energy efficiency as well as the performance of the SRM motor drive. This gives a preliminary estimation of the required battery size given the constraints in space and weight available in the vessel design.

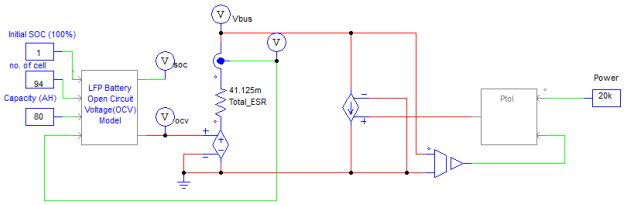

Fig.14 Battery discharging simulation schematics

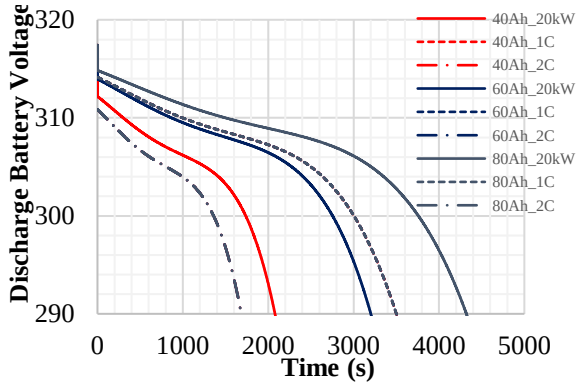

(a)

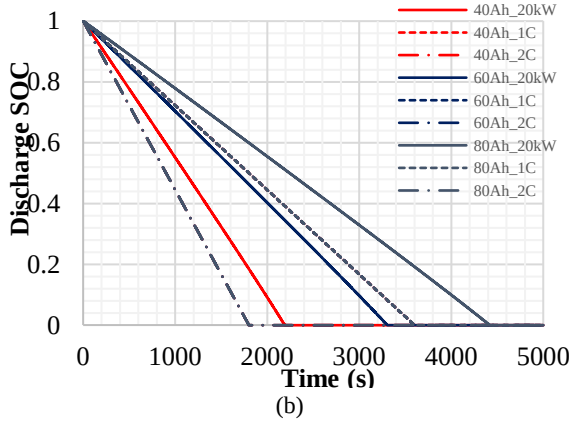

(b)

Fig.15 (a)Discharging battery voltage at different discharging current. (b)Discharging SOC at different discharging current.

TABLE 3: Design specification of battery module for electric vessel

Parameter	Value
Battery type	LiFePO4(LFP)
Nominal cell voltage	3.2V
Capacity	300V/80AH
Battery voltage range	290V to 312V
Charging cycle	>1000
Maximum discharging	150A
Casing	Stainless stell
IP rating	IP67
Module weight	140kg
Dimension	450*930*170 mm

VI. Conclusion and Future Works

This paper provides an electrification solution for a small waterjet engine vessel. A rigid and all insulated inductive wireless charger has been proposed to cater to the safer utilization and higher mobility of the mass on marine electrification. The wireless power transfer concept is adopted in the charging system but it is based on near flux power transfer. The top efficiency of the charger is 89.3% that is considered to be high for the subject. The coil and core are covered by the plastic shell and epoxy filler so that there is no metal or live component accessible. The LFP battery discharge simulation was conducted to validate the concept feasibility and high-efficiency operation. A vessel-based DC distribution system of 150V to power up the whole vessel is designed. All the components of a charger, motor drive, battery management, and control have been integrated into the e-vessel.

The future works include conducting a power test of the waterjet engine driven by SRM, to investigate the range speed and cruise speed. Development of a control algorithm of motor speed, torque relationship corresponding to the waterjet pressure head, mass flow to decrease the power density of the propulsion system for a higher speed. Considered the environmental protection, not only the assembly and integrated with flexible photovoltaic panels, even to explore the possibility of an unmanned marine vehicle is driven offshore PV generating field. It would be interesting to make the mobile generator and power bank based on E-vessel come reality.

Acknowledgment

The authors wish to acknowledge the support of the Innovation and Technology Funds under the project code ITS/073/18FP and the support provided by the members of the Power Electronics Research Centre (PERC), Department of Electrical Engineering, The Hong Kong Polytechnic University.

References

[1] O. L. Osen, "Optimizing electric energy production on-board offshore vessels: Vessel power consumption profile and production strategies using genetic algorithms," OCEANS 2016 - Shanghai, Shanghai, 2016, pp. 1-10, doi: 10.1109/OCEANSAP.2016.7485614.

[2] K. W. E. Cheng, X. D. Xue and K. H. Chan, "Zero emission electric vessel development," 2015 6th International Conference on Power

Electronics Systems and Applications (PESA), Hong Kong, 2015, pp. 1-5, doi: 10.1109/PESA.2015.7398965.

[3] International Convention for the Prevention of Pollution from Ships, 1973 as modified by the Protocol of 1978(MARPOL 73/78), International Maritime Organization, 1978.

[4] Jianping Bi, Xinli Wang and Lilin Li, "Diesel noise measurement and control of behavior analysis," 2011 Second International Conference on Mechanic Automation and Control Engineering, Hohhot, 2011, pp. 5730-5732, doi: 10.1109/MACE.2011.5988332.

[5] National Marine Fisheries Service, “Technical Guidance for Assessing the Effects of Anthropogenic Sound on Marine Mammal Hearing: Underwater Acouustic Threshoulds for Onset of Permanent and Temporary Threshould Shifts,” 2016.

[6] Roger W. Byard, Calle Winskog, Aaron Machado, Wayne Boardman, “The assessment of lethal propeller strike injuries in sea mammals, ” Journal of Forensic and Legal Medicine, Marine pollution bulletin, Vol.153, p.111031-111031, 2020-04.

[7] G. Guidi, J. A. Suul, F. Jenset and I. Sorfonn, "Wireless Charging for Ships: High-Power Inductive Charging for Battery Electric and Plug-In Hybrid Vessels," in IEEE Electrification Magazine, vol. 5, no. 3, pp. 22-32, Sept. 2017, doi: 10.1109/MELE.2017.2718829.

[8] Arash Eslamdoost, “Investigations of waterjet/hull interaction effects,” Ph.D. Thesis, Department of Shipping and Marine Techonology, Chalmers University Of Technology, Gothenburg, Sweden, 2012

[9] S. Elsaiah and C. Brady-Alvarez, "A Switched Reluctance Motor Drive System for Future Applications in the Emerged IMPS," 2018 North American Power Symposium (NAPS), Fargo, ND, 2018, pp. 1-5, doi: 10.1109/NAPS.2018.8600583.

[10] D Stapersma, Hk Woud, ”Matching propulsion engine with propulsor,” Journal of Marine Engineering & Technology, 4:2,pp. 25-32, 2005

[11] Z. Jin, G. Sulligoi, R. Cuzner, L. Meng, J. C. Vasquez and J. M. Guerrero, "Next-Generation Shipboard DC Power System: Introduction Smart Grid and dc Microgrid Technologies into Maritime Electrical Netowrks," in IEEE Electrification Magazine, vol. 4, no. 2, pp. 45-57, June 2016, doi: 10.1109/MELE.2016.2544203.

[12] Y. C. Fong, K. W. E. Cheng and R. Sekhar, "A Current Allocation Strategy Based Balancing Technique of Voltage Source String in Switch-Ladder Inverter and Its Switched-Capacitor Variety," in IEEE Transactions on Energy Conversion, doi: 10.1109/TEC.2020.3031224.

[13] Caihao Weng, Jing Sun and Huei Peng, ""A Current Allocation Strategy Based Balancing Technique of Voltage Source String in Switch-Ladder Inverter and Its Switched-Capacitor Variety," in IEEE Transactions on Energy Conversion," in dynamic systems and control conference, 2014

Key Technologies and New Developments of Stationary/Dynamic Wireless Power Transfer

Yong Li, Xiao Zhu, Min Zhang
School of Electrical Engineering, Southwest Jiaotong University, Chengdu, China
E-mail: yong_li@swjtu.edu.cn

Abstract – In the last few decades, wireless power transfer (WPT) is widely used in various applications due to its safety and reliability, and has become the trend of power supply in the future. However, there are still some challenges and problems to be solved in practical applications, such as large current stress with single phase-shift control, multiple outputs for driving multi-string LEDs, power pulsation phenomenon or power null phenomenon in dynamic WPT (DWPT) system. This tutorial will introduce these problems and present the corresponding solutions in detail.

Keywords - Wireless power transfer (WPT), multiple outputs, current stress, power pulsation phenomenon, power null phenomenon.

I. INTRODUCTION

The technology of wireless power transfer (WPT) originated in the late 19th century. In 1893, Nikola Tesla put forward the concept of WPT and light a bulb without any wire connection. For over hundred years, the United States and other countries have carried out research on WPT. Since the beginning of the 21st century, the WPT technology has made a breakthrough. In 2007, Marin Soljacic, the professor of Massachusetts Institute of Technology (MIT), and his team lighted a 60W bulb at a distance of more than 2m with 40% efficiency by using the principle of magnetic resonance coupling [1].

WPT can be classified into the following three types: radiative power transfer, capacitively coupled power transfer (CCPT) and inductive power transfer (IPT). Among them, radiative power transfer is widely used in medical and military fields due to its good directivity and long transfer distance. In contrast, CCPT transmission distance is limited so that it is often used for short distance charging. Compared with the above two types, IPT is a hot topic in current research because of its stability, convenience and effectiveness. It should be noted that, in this tutorial, the WPT system refers to the IPT system [2].

WPT technology has been successfully applied in portable electronic devices, medical electronic devices, household appliances, electric vehicles, rail traffic, etc. For a typical WPT system shown in Fig. 1, a full-bridge inverter is used to convert the DC source to high-frequency current in the primary side, which will generate an induced voltage in the secondary side through the magnetic coupler. The induced voltage can be converted to DC source by the rectifier for supplying the load. To maximize the transmission efficiency and power capacity, the compensation network should be installed between the converter and the coupler [3].

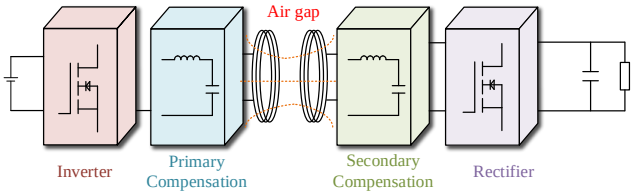

Fig. 1. A typical WPT system.

In recent years, with the in-depth research of the WPT system, this technology has made a great breakthrough. However, there are still some challenges and problems to be solved. Section II will present a method to optimize the current stress [4]. Section III will introduce two topologies to achieve multiple load-independent outputs for driving multiple LEDs [5],[6]. Section IV will present a magnetic coupler design method for dynamic charging of EVs [7]. Finally, a summary and conclusion will be shown in Section V.

II. CURRENT-STRESS ISSUES AND OPTIMIZATION

Generally, in some applications, the equivalent resistance of the load varies in a wide range. For example, the resistance of the battery will vary during the charging process. Besides, it is preferable for battery charging in two modes to increase its service life and safety: 1) Constant current (CC) mode; 2) Constant voltage (CV) mode. The conventional single-phase-shift (SPS) control can achieve the desired output current or voltage by adjusting the conduction angle of the inverter in the primary side. However, the unbalanced current-stress will exist when the load varies. This will result in two consequences: high devices costs and low system efficiency. For one thing, the need of the devices with high volt-ampere rating will increase due to the unbalanced current, which will obviously make a higher cost. For another, excessive current will lead to the higher switching losses and component losses so that the efficiency is reduced. Moreover, the devices may also be damaged due to the excessive voltage stress on compensation capacitors and coupler coils [4].

To solve this problem, a control method using dual-phase-shift (DPS) is proposed, which can not only ensure the constant output of the system, but minimize the current stress on both sides by regulating the active inverter and rectifier [4]. The circuit diagram of DPS control is shown in Fig. 2.

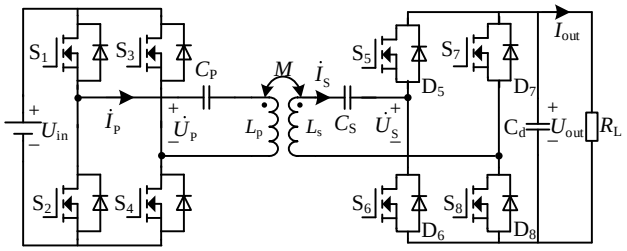

Fig. 2. Circuit diagram of the WPT system for the proposed DPS control [4].

By using the Kirchhoff Voltage Law (KVL) and fundamental harmonic approximation (FHA) method, the relationships between the voltages and currents are

$$\begin{cases} \dot{U}_{\mathrm{P}} = j\omega M\dot{I}_{\mathrm{S}} = \dfrac{2\sqrt{2}U_{\mathrm{in}}}{\pi}\sin\dfrac{\alpha}{2} \\ \dot{U}_{\mathrm{S}} = j\omega M\dot{I}_{\mathrm{P}} = j\dfrac{2\sqrt{2}kU_{\mathrm{in}}}{\pi}\sin\dfrac{\beta}{2} \end{cases} \tag{1}$$

where α, β are the conducting angle of inverter and rectifier respectively, and k is the voltage conversion ratio calculated by $k=U_{\mathrm{out}}/U_{\mathrm{in}}$. Thus, one can obtain

$$\begin{cases} \dot{I}_{\mathrm{S}} = \dfrac{\dot{U}_{\mathrm{P}}}{j\omega M} = -j\dfrac{2\sqrt{2}U_{\mathrm{in}}}{\omega M\pi}\sin\dfrac{\alpha}{2} \\ \dot{I}_{\mathrm{P}} = \dfrac{\dot{U}_{\mathrm{S}}}{j\omega M} = \dfrac{2\sqrt{2}kU_{\mathrm{in}}}{\omega M\pi}\sin\dfrac{\beta}{2} \end{cases} \tag{2}$$

Furthermore, both the input power and output power can be obtained when the coil resistances are ignored

$$P_{\mathrm{O}} = P_{\mathrm{in}} = \mathrm{Re}(\dot{U}_{\mathrm{P}}\cdot\dot{I}_{\mathrm{P}}^{*}) = \mathrm{Re}(\dot{U}_{\mathrm{S}}\cdot\dot{I}_{\mathrm{S}}^{*}) = \frac{8}{\pi^2}\frac{kU_{\mathrm{in}}^{2}}{\omega M}\sin\frac{\alpha}{2}\sin\frac{\beta}{2} \tag{3}$$

In order to minimize the current stress of both transmitter and receiver when delivering the same power, $I_{\mathrm{P}}=I_{\mathrm{S}}$ should be satisfied, i.e.,

$$\alpha = 2\arcsin\left(k\sin\frac{\beta}{2}\right) \tag{4}$$

Substituting (4) into (3), the output power can be calculated as

$$P_{\mathrm{O}} = \frac{8}{\pi^2}\frac{k^2U_{\mathrm{in}}^{2}}{\omega M}\sin^2\frac{\beta}{2} \tag{5}$$

According to (5), the desired output power can be realized by adjusting β. According to (4), the value of α varies with β. Thus, the control strategy diagram could be shown as Fig. 3.

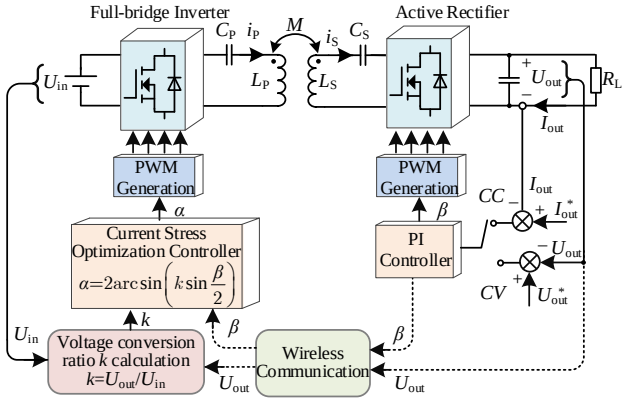

Fig. 3. Control strategy of DPS method [4].

To verify the validity of the proposed DPS control method, an experimental prototype is established. The results of current stress and efficiency are shown in TABLE I and Fig. 4.

TABLE I
EXPERIMENTAL RESULTS [4]

Control methods	Output power	Output voltage	Transmitter current	Receiver current	Maximum current
The SPS control	350W	150V	9A	4A	9A
		200V	12A	3A	12A
		250V	15A	3A	15A
	500W	150V	10A	8A	10A
		200V	12A	5A	12A
		250V	12A	4A	12A
The proposed control	350W	150V	6A	6A	6A
		200V	6A	6A	6A
		250V	6A	6A	6A
	500W	150V	8A	8A	8A
		200V	7A	7A	7A
		250V	6A	6A	6A

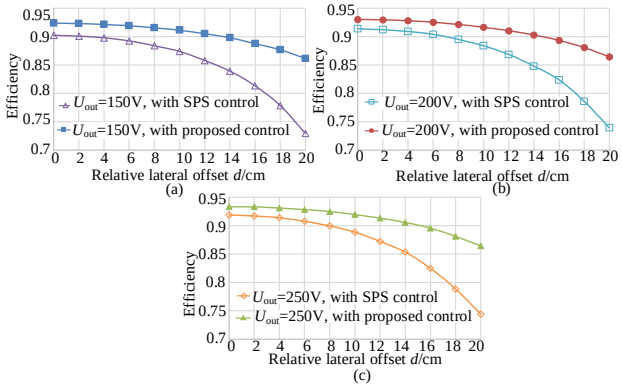

Fig. 4. Overall system efficiency comparison between the DPS control and the SPS control against different misalignments [4].

Great agreement is obtained between the experimental results and theoretical analysis according to TABLE I, and it is verified that the proposed DPS control method can reduce the current stress on both sides effectively. Thus, the efficiency of the system is improved.

III. MULTI-OUTPUT SYSTEM FOR DRIVING LEDS

LEDs driving is also an important application of the WPT technology. Practically, there are two requirements should be considered. Firstly, to fulfill the requirement of the high light intensity, multiple LED strings are connected in parallel. That means, LED strings need to be driven simultaneously, and the driver should achieve multiple output channels. Furthermore, the luminosity of a LED depends on its forward current. Thus, the preferable driving method is CC supply. In order to satisfy the requirements, reference [8] has proposed a WPT system with multiple receivers. However, the following drawbacks are inevitable: 1) The number of receivers equals the number of loads, resulting in increased installation space and system costs; 2) Each receiver is expected to have the same size and identical mutual inductance, which is difficult to achieve in practice.

To realize these two requirements simply and feasibly, a WPT system with only one receiver and multiple constant current outputs is proposed for supplying LED strings [5]. The circuit diagram of multi-channel WPT system is shown in Fig. 5.

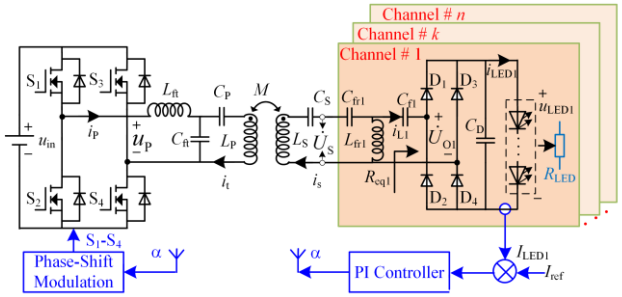

Fig. 5. Diagram of multi-channel WPT system and control strategy for supplying LED strings [5].

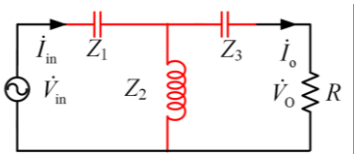

Fig. 6. T-CLC resonant circuit [5].

It can be found from Fig. 5, CV output characteristic can be achieved for LCL-S topology according to [9], the output voltage can be calculated as

$$\dot{U}_S = \frac{\dot{U}_P M}{L_{ft}} = \frac{2\sqrt{2}U_{in}M}{\pi L_{ft}} \sin\frac{\alpha}{2} \tag{6}$$

where α is the conduction angle of the inverter. For T-CLC resonant circuit shown in Fig. 6, we can get the following relationship by KVL

$$\begin{cases} \dot{I}_o = -\dfrac{1}{Z_2}\dot{V}_{in} \\ \dot{V}_o = Z_2 \dot{I}_{in} \\ Z_{in} = \dfrac{\dot{V}_{in}}{\dot{I}_{in}} = -\dfrac{Z_2^{\,2}}{R} \end{cases} \tag{7}$$

It is obvious that the T-CLC resonant can be considered as a CC source for driving LED strings when the input source is a CV source. Furthermore, the input impedance is purely resistive, which means the zero-phase-angle (ZPA) operation can be achieved.

It is worth emphasized that the output current ratio of each channel is equal to the corresponding parallel inductance inverse ratio, i.e.,

$$\frac{I_{LEDk}}{I_{LED(k+1)}} = \frac{L_{fr(k+1)}}{L_{frk}} \tag{8}$$

From (8), the output current is not related to the load of each other, which means the current in one channel can be adjusted independently without considering the effect on the other channels.

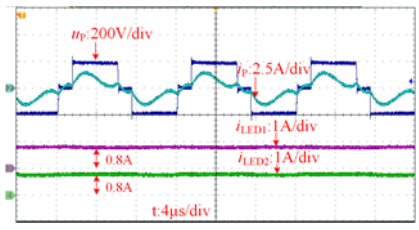

Fig. 7. The waveforms of u_P, i_P, i_{LED1} and i_{LED2} when the reference current is 0.8A [5].

A laboratory prototype with dual independent output currents is built. The results of steady and dynamic performances are shown in Fig. 7 and Fig. 8 respectively.

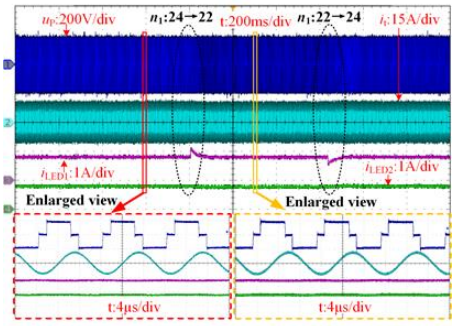

Fig. 8. The dynamic response of the proposed system[5].

The experimental results have verified that each LED string can be driven stably at corresponding desired current.

Furthermore, another cost-effective method with three coils to realize multiple outputs for LEDs driver is presented in [6]. Unlike the method proposed in [5], a three-coil WPT system is more energy efficient with extended transfer distance. In order to further save the install space, the T-circuit is designed as magnetically integrated LCL resonators shown in Fig. 9.

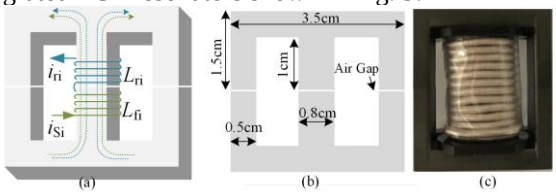

Fig. 9. (a) structure of inductors; (b) sizes of the inductor core from a front view; (c) the implementation of the coupled inductor [6].

IV. Coil Design For the DWPT

Compared to stationary WPT, the DWPT technology seems to be a promising solution for EVs charging due to the cost and capacity reduction of the on-board batteries. The transmitter structure design of DWPT can be divided into the followings: 1) the long-track-loop type; 2) the multiple-individual-transmitter type. However, because of the larger AC resistance and electromagnetic interference (EMI), the applications of this type are limited. For the second type, despite of its many advantages, such as manufactured modularly, flexible, energy-saving. There are still some critical issues that need to be solved. One is the power pulsation phenomenon due to the frequent variation of *M*. A method by adjusting the distance between adjacent transmitters is proposed in [10], but the reduction of track length and the design complexity of compensation networks seem to degrade the performance of the whole system. The proposed methods are to use an additional compensation in [11]-[13]. However, the extra power loss and high current stress indicates that the method is less feasible. Depending on the DDQ structure design for receiver seems to be a method of eliminating power null phenomenon. However, the power pulsation phenomenon still exists [14].

To address the mentioned issues, a new coil structure design proposed in [7] is shown in Fig. 10. For this structure, the transmitter is composed of DD coil and Q coil arranged alternately, and the receiver is composed of DD coil and Q coil in series.

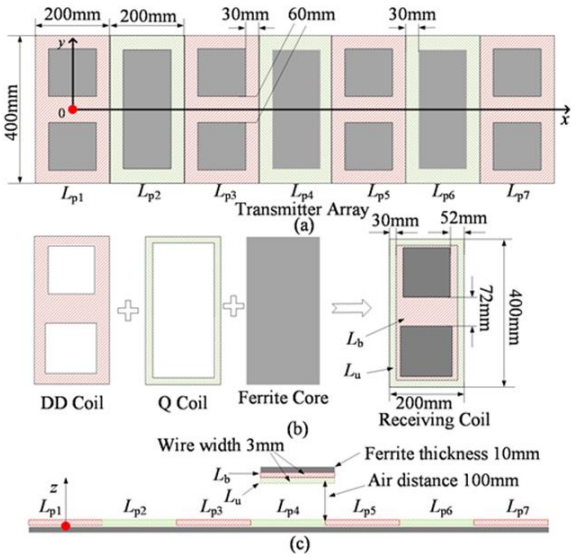

Fig. 10. (a) the structure and size of transmitter array, (b) the structure and size of receiver coil, (c) the proposed coupler [7].

Using ANSYS Maxwell, the simulated results shown in Fig. 11 and Fig. 12 indicate that the mutual inductance between adjacent transmitters is equal to zero approximately, and the mutual inductance between two sides is constant. Obviously, this structure has a good performance for DWPT.

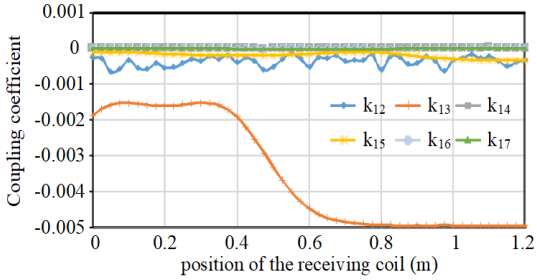

Fig. 11. Diagram of coupling coefficients between transmitter coil #1 and other transmitters [7].

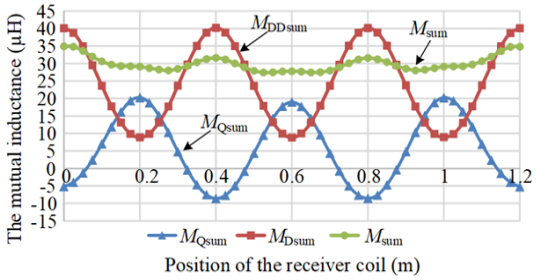

Fig. 12. Waveform of mutual inductance at dynamic condition [7].

To reduce EMI, the segmentation control is proposed, i.e., when the coils are aligned, three transmitters work, when the coils are offset, four transmitters work. For requirements of CC and CV charging, the change of compensation network method is used and shown in Fig. 13. When S_1 is ON and S_2 is OFF, the compensation network is LCL-LCL, so that the system is working in CC mode. When S_1 is OFF and S_2 is ON, the compensation network is LCL-S, so that the output voltage is constant and the system is working in CV mode [9].

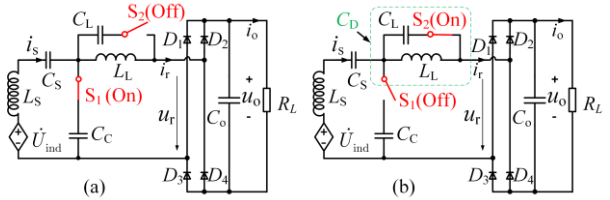

Fig. 13. The circuit diagram of the receiver side under different charging modes controlled by S_1 and S_2. (a) CC mode and (b) CV mode [7].

A laboratory setup with seven transmitters is built, and the results are shown in Fig. 14. The experimental results have demonstrated that the CC and CV charging can be well achieved for DWPT with high efficiency.

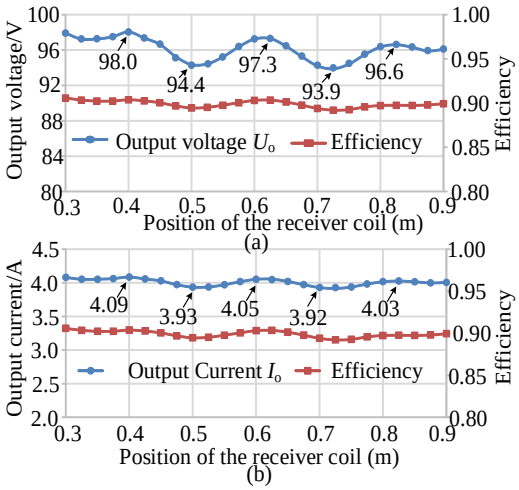

Fig. 14. The waveforms of outputs and efficiency when receiver coil at different position. (a) CV mode, (b) CC mode [7].

V. Summary And Conclusion

This tutorial introduced and solved three common problems in WPT applications: 1) realizing the current-stress optimization with DPS control for battery charging; 2) realizing multiple outputs by T-resonant circuit for LEDs driving; 3) eliminating the power null phenomenon and power pulsation phenomenon with coil design for EVs dynamic charging. The experimental results show that these methods are feasible and effective.

Certainly, the challenges and problems in practical applications for the WPT are far more than these. The future work will be to research the problems which have not yet been solved.

Acknowledgment

This work was supported in part by the National Natural Science Foundation of China under Grant 51907169, in part by the Sichuan Science and Technology Program under Grant 2020YFH0031.

The authors would also be grateful to the Organization Committee of the 2020 8th International Conference on Power Electronics Systems and Applications, IEEE, Hong Kong Polytechnic University, China for inviting this tutorial paper.

References

[1] A. Kurs, A. Karalis, R. Moffatt, et al., "Wireless Power Transfer via Strongly Coupled Magnetic Resonances," Science, vol. 317, no. 5834, pp. 83-86.

[2] H. Feng, R. Tavakoli, O. C. Onar and Z. Pantic, "Advances in High-Power Wireless Charging Systems: Overview and Design Considerations," in *IEEE Transactions on Transportation Electrification*, vol. 6, no. 3, pp. 886-919, Sept. 2020, doi: 10.1109/TTE.2020.3012543.

[3] S. Li, W. Li, J. Deng, T. D. Nguyen, and C. C. Mi, "A double-sided LCC compensation network and its tuning method for wireless power transfer," *IEEE Trans. Veh. Technol.*, vol. 64, no. 6, pp. 2261–2273, Jun. 2015.

[4] Y. Li, J. Hu, F. Chen, Z. Li, Z. He and R. Mai, "Dual-Phase-Shift control scheme with current-stress and efficiency optimization for wireless power transfer systems," in *IEEE Transactions on Circuits and Systems I: Regular Papers*, vol. 65, no. 9, pp. 3110-3121, Sept. 2018.

[5] Y. Li, J. Hu, X. Li, F. Chen, Q. Xu, R. Mai, Z. He, "analysis, design, and experimental verification of a mixed high-order compensations-based WPT system with constant current outputs for driving multistring LEDs," in *IEEE Transactions on Industrial Electronics*, vol. 67, no. 1, pp. 203-213, Jan. 2020.

[6] Y. Li, J. Hu, X. Li, H. Wang and K. W. E. Cheng, "cost-effective and compact multistring LED driver based on a three-coil wireless power transfer system," in *IEEE Transactions on Power Electronics*, vol. 34, no. 8, pp. 7156-7160, Aug. 2019.

[7] Y. Li, J. Hu, T. Lin, X. Li, F. Chen, Z. He, R. Mai, "a new coil structure and its optimization design with constant output voltage and constant output current for electric vehicle dynamic Wireless Charging," in *IEEE Transactions on Industrial Informatics*, vol. 15, no. 9, pp. 5244-5256, Sept. 2019.

[8] M. Liu, M. Fu, and C. M, "Battery cell equalization via megahertz multiple-receiver wireless power transfer," in *IEEE Trans. Power Electron*., vol. 33, no. 5, pp. 4135–4144, May. 2018.

[9] Fang Liu, Y. Zhang, K. Chen, Z. Zhao and L. Yuan, "A comparative study of load characteristics of resonance types in wireless transmission systems," *2016 Asia-Pacific International Symposium on Electromagnetic Compatibility (APEMC)*, 2016, pp. 203-206.

[10] M. Yang, Y. Li, R. Mai, B. Wang, and Z. He. "Determining coil distance of cross-segmented IPT system for constant output voltage," *Applied Power Electronics Conference and Exposition (APEC)*, 2017, pp. 1401-1406.

[11] Y. L. Li, Y. Sun, and X. Dai. "μ-synthesis for Frequency Uncertainty of the ICPT System." in *IEEE Trans. Ind. Electron.*, vol. 60, no. 1, pp. 291–300, Jan. 2013.

[12] F. Pijl, M. Castilla, P. Bauer, "Adaptive slide-mode control for a multiple-user inductive power transfer system without need for communication," in *IEEE Trans. Ind. Electron.*, vol. 60, pp. 271-279, 2013.

[13] A. Ong, P. Sampath, J. H. Cheong, "transmitter pulsation control for dynamic wireless power transfer systems," in *IEEE Trans. Transport. Electrific.*, vol. 3, no. 2, pp. 418-426, May 2017.

[14] S. Zhou and C. Mi, "Multi-paralleled LCC reactive power compensation networks and their tuning method for electric vehicle dynamic wireless charging," in *IEEE Trans. Ind. Electron.*, vol. 63, no. 10, pp. 6546–6556, Oct. 2016.

Author Index

Submission Details

Only online submission will be accepted. Please first register and submit online. The paper is in double-column and is similar to most IET or IEEE journal formats. There is no page limit. Any number of pages of more than 6 will be subjected to an additional charge.

The paper guidelines can be downloaded using the link: http://perc.polyu.edu.hk/apejournal/

Any queries, please contact Prof. Eric Cheng, Publishing Director of APEJ, Dept. of Electrical Engineering, The Hong Kong Polytechnic University, Hung Hom, Hong Kong. Email: eeecheng@polyu.edu.hk Fax: +852-2330 1544

Any secretarial support and production related matters, please contact Dr. James Ho, Power Electronics Research Centre, The Hong Kong Polytechnic University, Hung Hom, Hong Kong. Email: eeapej@polyu.edu.hk Tel: +825-3400 3348 Fax: +852-3400 3343

Publication Details

The journal will be published 2-3 times a year. The first issue was published in 2007. Response time for paper acceptance is within 3 months.

Financial Charge

All the accepted papers will be printed without charge for 6 or less pages. An additional page charge is HK$100 per page. A hardcopy of the journal will be posted to the corresponding author free of charge. Additional copies of the journal can be purchased at HK$200 each. The charge includes postage and packing.

All Chinese Papers will be subjected to a translational fee of HK$350 per page. It will be charged when the paper is accepted for publication.

Advertising

Advertisement is welcome. Full page advertisement is HK$1000. For colour advertisements, the amount is doubled. All the advertisements will be both posted online in the journal website and hardcopy of the journal.

For advertising enquires and details, please contact Ms. Anna Chang, eeapej@polyu.edu.hk.

Tel: +852-3400 3348, Fax: +852-3400 3343

For payment, please send your cheque, payable to ‘The Hong Kong Polytechnic University, address to Ms. Kit Chan, Secretary of APEJ, Dept. of Electrical Engineering, The Hong Kong Polytechnic University, Hung Hom, Hong Kong.’